Cent. Eur. J. Phys. • 7(1) • 2009 • 89-95
DOI: 10.2478/s11534-008-0147-5

VERSITA

Central European Journal of **Physics**

Structural and magnetic characterisation of the perovskite oxides $La_{0.7}Ca_{0.3-x}Na_xMnO_3$

Research Article

Anowar Tozri[1]*, Moez Bejar[1], Essebti Dhahri[1]†, EL Kébir Hlil[2]

1 *Laboratoire de Physique Appliquée, Faculté des Sciences de Sfax, B.P 802, Sfax 3018 Tunisie*

2 *Laboratoire de Cristallographie, CNRS, 25 avenue des Martyrs, B.P 166, 3804 Grenoble Cedex 9 France*

Received 25 August 2008; accepted 6 November 2008

Abstract: X-ray powder diffraction (XRD) and magnetic measurements were performed in order to investigate the effect of Na^+ ion substitution for Ca^{2+} ions on the crystallographic structure, the character of magnetic ordering, and the effect of transition temperature in $La_{0.7}Ca_{0.3-x}Na_xMnO_3$ manganites series ($0 \leqslant x \leqslant 0.2$). All samples crystallise in an orthorhombic structure with the *Pnma* space group. We have found a strong dependence of structural and magnetic properties on the cation-size disorder parameter σ^2. The temperature dependence of magnetization of all samples obeys the Bloch $T^{3/2}$ law. The values of the spin wave constant at low temperature B increase with the increase of x and the Curie temperature decreases. It is concluded that the substitution of Ca by Na^+ ions causes a decrease in total exchange integral $A$of the samples.

PACS (2008): 71.70.Gm, 74.25.Ha, 75.30.Ds, 75.30.Cr, 75.47.Lx

Keywords: manganites • Jahn-Teller effect • charge-ordered • ferromagnetic • cation-size disorder

1. Introduction

The systematic investigation of the phase diagram of the perovskite manganites was initially performed on $La_{1-x}Ca_xMnO_3$ in fiftieth [1, 2]. After the discovery of the colossal magnetoresistance (CMR) effect in the doped perovskite manganites $R_{1-x}A_xMnO_3$ (R: rare – earth, A: alkali – earth elements) these materials became a popular subject because of their fascinating physical properties such as competing magnetic order, metal – insulator transitions and charge/orbital ordered (CO – OO) [3, 4] states observed in doped manganites. The system offers a high degree of chemical flexibility. This leads, together with a complex interplay between structures, electronic and magnetic properties, to very rich phase diagrams involving various metallic, insulating and magnetic phases [4–6]. These properties are sensitive to doping concentration x, average cationic radii $\langle r_A \rangle$, and mismatch in ionic radii $\sigma^2 = \sum_i (x_i r_i^2 - \langle r_A \rangle^2)$, where x_i and r_i are the atomic fraction and ionic radii of i-type ions at A site, respectively.

It is well known in the manganites exhibiting CMR, the ferromagnetic T_C increases with the average radius $\langle r_A \rangle$

*E-mail: Tozri_anowar@yahoo.fr
†E-mail: essebti@yahoo.fr

and the charge ordering transition is also highly sensitive to $\langle r_A \rangle$ and T_{CO} increases with the decrease of $\langle r_A \rangle$.

A larger $\langle r_A \rangle$ enhances the bandwidth of the e_g electron in Mn ion which favours double exchange (DE) interaction between Mn^{3+} and Mn^{4+} through the bridging of oxygen ions. This stabilizes the ferromagnetic metallic phase at low temperatures. The conductivity in the ferromagnetic metallic state is explained by Zener's double exchange mechanism [3–7]. Lower values of $\langle r_A \rangle$ result in narrow e_g electron bandwidth. In this case, the kinetic energy of itinerant e_g electron is not high enough to enable a charge delocalization. Hence these systems may achieve a charge – ordered (CO) antiferromagnetic (AFM) ground state which is electrically insulating [8] or ferromagnetic insulating ground state [9].

Previous studies [10–14] showed that the A – site cational size mismatch can lead to random local lattice distortion. In Tomioka and Tokura's study, they found that the A – site disorder has great effects on the properties of manganites and gave the phase diagram of disorder versus $\langle r_A \rangle$ [12], also many studies [15, 16] showed that T_C has been related to the variance in the distribution of $\langle r_A \rangle$ and the T_C decreases significantly with the variance, σ^2 based on the studies of manganites with fixed $\langle r_A \rangle$. A similar study of the variation of T_{CO} with σ^2 in $Ln_{0.5}A_{0.5}MnO_3$ for fixed $\langle r_A \rangle$ values of 1.17 Å and 1.24 Å has shown that T_{CO} is not sensitive to the size mismatch σ^2 [17].

The Jahn – Teller effects [18] and Coulomb interactions play an important role in these systems which results in the distortion of Mn – O octahedra determining the nature of the CO state in these materials [19].

Polycrystalline $La_{0.7}Ca_{0.3}MnO_3$ sample in $La_{0.7}Ca_{0.3-x}Na_xMnO_3$ series shows the FM-PM transition which motivated us to investigate this sample elaborately. We, therefore, took the $La_{0.7}Ca_{0.3}MnO_3$ as the base sample and replaced Ca by Na to study the effect of the couple ($\langle r_A \rangle$, σ^2) on different characteristics.

2. Experimental details

Polycrystalline $La_{0.7}Ca_{0.3-x}Na_xMnO_3$ ($0 \leqslant x \leqslant 0.2$) samples were prepared by Sol-gel method. Appropriate proportions of high purity La_2O_3, $CaCO_3$, Na_2CO_3 and $Mn(NO_3)_2$, $4H_2O$ were dissolved in dilute HNO_3 solution at 333 K. Suitable amounts of citric acid and ethylene glycol as coordinate agents were added and a complete homogenous transparent solution was achieved. This solution was subjected to a slow evaporation at 333 K until a high viscous residual was formed and a gel was developed during heating at 443 K. The gel was thermally treated at 873 K for 5 hours for the purpose of organic precursor decomposition. After grinding, the samples were calcinated in air at 1273 K for 5 hours. The structure and phase purity of the prepared samples was checked by powder X-ray diffraction (XRD), using Cu K_α radiation by step scanning (0.02°) at room temperature. Refinements of the XRD data were carried out with the Rietveld refinement using the program FULLPROF [20]. The microstructure and elemental distribution of the samples were studied in a 5410 LV Jeol scanning electron microscope (SEM), which includes an energy dispersion spectrometer (EDS). Magnetization measurements versus temperature in an applied field of 500 Oe were recorded using a Foner magnetometer (FON) equipped with a superconducting coil between 10 K and 300 K.

3. Results and discussion

Fig. 1 shows SEM photographs of some representative sample (x = 0.1 – Fig. 1a, x = 0.15 – Fig. 1b and the crystallites are homogenous and small in the range of 1.01 μm – 1.23 μm. From the EDS spectrum of $La_{0.7}Ca_{0.3-x}Na_xMnO_3$, one can see that there are no impurities and the sample composition is similar to the nominal one.

The XRD patterns of $La_{0.7}Ca_{0.3-x}Na_xMnO_3$ ($0 \leqslant x \leqslant 0.2$) samples at room temperature clearly indicates a single phase with no detectable secondary phase. The positions of different peaks do not change much with the alteration of Na concentration confirming the unaffected structure of the system. The diffractograms can be indexed based on orthorhombically distorted perovskite structure. The Rietveld refinements were carried out in the Pnma space group. We represented in the Fig. 2 the diffractograms for x = 0.05 and x = 0.2. The refinement results are listed in Tab. 1.

We can first see from the variation of the cell volume and the lattice parameters $\left(a,\ b/\sqrt{2} \text{ and } V\right)$ represented in Fig. 2, that the sample with x= 0 exhibits a symmetry orthorhombic (O) defined by $\left(a < b/\sqrt{2}\right)$ with changes of one symmetry orthorhombic (O') defined by $\left(a > b/\sqrt{2}\right)$ for x⟩0. Secondly, this variation presents a minimum for x = 0.1 in the unit cell volume and for the cell parameters. This variation is not in agreement with the increase of Na which leads to an increase of $\langle r_A \rangle$ due to the difference in ionic radii of Ca^{2+} $\left(\langle {}^{IX}r_{Ca^{2+}} \rangle = 1.18 \text{ Å}\right)$ and Na^+ $\left(\langle {}^{IX}r_{Na^+} \rangle = 1.24 \text{ Å}\right)$ [21]. This suggests that $\langle r_A \rangle$ is not the essentially responsible for the change of the structural parameter for this system.

This unexpected result suggests that size differences between the different cations located in the A-site must be taken into consideration, as it is known, larger value of σ^2

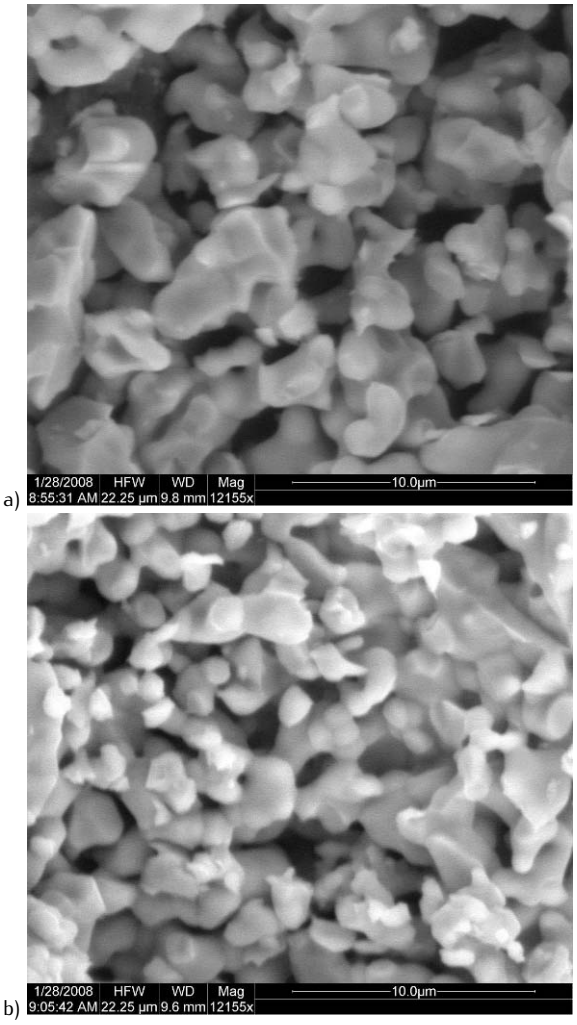

Figure 1. SEM photographs of $La_{0.7}Ca_{0.3-x}Na_xMnO_3$ with x = 0.1 and x = 0.15.

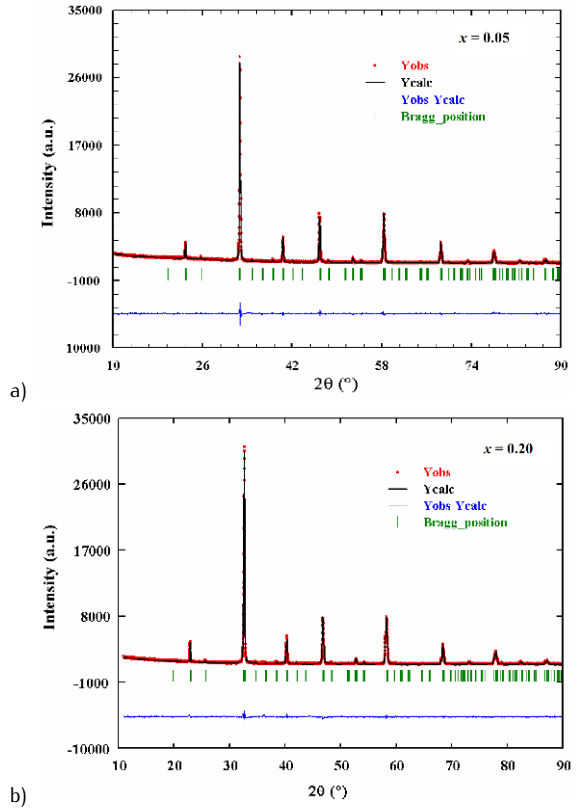

Figure 2. Observed (circle), calculated (continuous line) and difference patterns (at the bottom) of X-ray diffraction data fitted with orthorhombic structure (*Pnma*) in $La_{0.7}Ca_{0.3-x}Na_xMnO_3$ compounds: a) x = 0.05; b) x = 0.20. The vertical tick indicates the allowed reflections. We notice that calculated diffraction patterns match well with the measured ones.

implies higher degree of disorder and so a higher degree of structural distortion. To affirm this result, we have calculated the values of the lattice constant, quantity $D_O(\%)$ characterizing the orthorhombic deformation, which can be written as

$$D_O = \frac{1}{3}\sum_{i}^{3}\left|\frac{a_i - \bar{a}}{\bar{a}}\right| \times 100 \qquad (1)$$

where $a_1 = a$, $a_2 = c$ and $a_3 = b/\sqrt{2}$, and $\bar{a} = \left(abc/\sqrt{2}\right)^{\frac{1}{3}}$.

And σ_{JT}^2 characterizing the MnO_6 distortion and quantified using the Jahn – Teller distortion, can be written as

$$\sigma_{JT} = \sqrt{\frac{1}{3}\sum_{i}^{3}\left[(Mn-O)_i - \langle Mn-O\rangle\right]^2} \qquad (2)$$

i.e. that the σ^2 and ($D_O(\%)$, σ_{JT}^2) parameters are of different origins, the first is deducted from the value of $\langle r_A\rangle$ and the second are the result of the refinement Rietveld. The values of these three parameters are listed in Tab. 2.

From Fig. 3 we can see the same variation for these three parameters, we note that the variation of σ^2 for the system $La_{0.7}Ba_{0.3-x}Na_xMnO_3$ [22] et $La_{0.7}Ca_{0.3-x}K_xMnO_3$ [23] is not the same observed for our system and also the sample with x = 0.1 has the highest value of σ^2 that maintains elevated values of orthorhombic deformation $D_O(\%)$ and Jahn-Teller distortion σ_{JT}^2. Hence higher degree of disorder induces higher degree of structural distortion which induces the minimum of the cell volume. Hence, it can be seen in the $La_{0.7}Ca_{0.3-x}Na_xMnO_3$ system that the variance σ^2 controls the structural distortion and as a result

Table 1. Crystallographic data for $La_{0.7}Ca_{0.3-x}Na_xMnO_3$ compounds with $0.0 \leqslant x \leqslant 0.20$ form the Ritveld refinement of X-ray diffraction data.

Crystallographic data	$x = 0.00$	$x = 0.05$	$x = 0.10$	$x = 0.15$	$x = 0.20$
a (Å)	5.4811_3	$5,4663_2$	$5,4613_0$	5.4730_1	5.4740_6
b (Å)	7.7622_3	$7,7274_1$	$7,7185_0$	7.7366_1	7.7384_8
c (Å)	5.4744_7	$5,4860_4$	$5,4792_1$	5.4963_5	5.5031_8
V (Å^3)	58.229_1	$57,933_0$	$57,741_5$	58.182_4	58.280_1
La, Ca, Na x	0.0158	0.0192	0.0189	0.0182	0.0152
Z	-0.0065	-0.0042	-0.0046	-0.0037	-0.0007
O(1) x	0.5220	0.4980	0.4924	0.4943	0.4864
Z	0.0469	0.0560	0.0510	0.5030	0.0403
O(2) x	0.7837	0.2783	0.2554	0.2704	0.2822
Y	0.0386	0.0351	0.0613	0.0313	0.0291
Z	0.7961	0.7504	0.7103	0.7102	0.6986
Mn-O1 × 2 (Å)	1.961_2	1.956_3	1.950_2	1.954_2	1.949_2
Mn-O2 × 2 (Å)	1.991_2	2.065_0	2.131_1	2.045_1	2.056_1
Mn-O2 × 2 (Å)	1.917_4	1.851_0	1.868_1	1.891_1	1.905_1
⟨Mn-O⟩	1.956_6	1.957_4	1.983_1	1.963_4	1.970_1
Mn-O1-Mn (°)	163.37	161.92	163.32	163.71	166.26
Mn-O2-Mn (°)	160.22	162.88	155.68	160.37	157.04
⟨Mn-O-Mn⟩	161.79	162.4	159.5	162.04	161.65
R_P	5.78	2.23	2.71	2.27	2.02
R_{WP}	7.30	2.89	3.78	3.06	2.60
χ^2	0.92	1.38	2.26	1.56	1.24

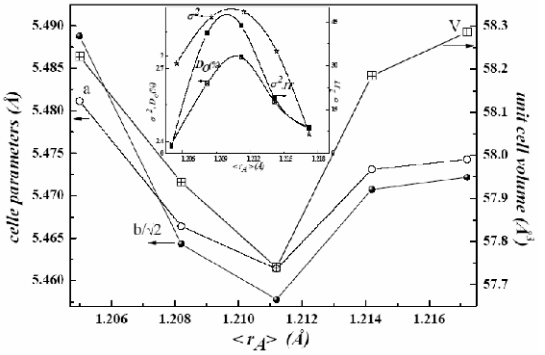

Figure 3. Variation of the cell parameters and the unit cell volume V as a function of the ionic radii $\langle r_A \rangle$ for $La_{0.7}Ca_{0.3-x}Na_xMnO_3$ compounds. Inset show the variation of σ^2, $D_O(\%)$ and σ^2_{JT} as function of the ionic radii $\langle r_A \rangle$.

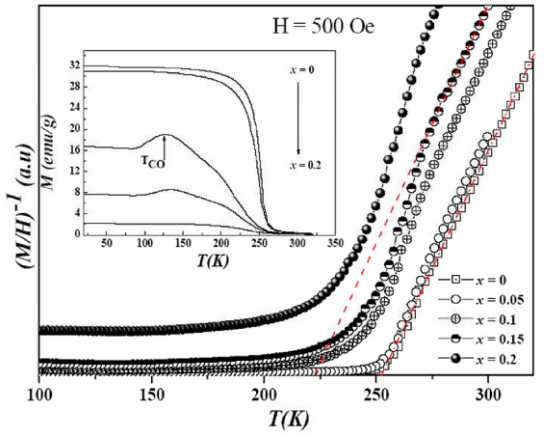

Figure 4. Inverse susceptibility (defined as $(M/H)^{-1}$) of the $La_{0.7}Ca_{0.3-x}Na_xMnO_3$ samples. Curie temperatures were deduced by extrapolation of linear parts of the susceptibility curves as shown for x = 0 and x= 0.15. Inset show the temperature variation of magnetization of $La_{0.7}Ca_{0.3-x}Na_xMnO_3$ samples.

the variation of the cell volume is inversely proportional to variation of the structural distortion.

Fig. 4 shows the temperature dependence of the inverse low-field susceptibility for the $La_{0.7}Ca_{0.3-x}Na_xMnO_3$ compounds as calculated from magnetization data. Here the susceptibility is defined as $(M/H)^{-1}$ (the susceptibility is usually defined as M/H, where M is the magnetization per volume). The high-temperature part of the magnetization curves follows Curie – Weiss law, indicating paramagnetic materials at this temperature range. The Curie temperature were determined by extrapolating the paramagnetic part of the inverse susceptibility, as shown for x = 0 and x= 0.2. This was done by linear regression with an error of ±3 K. From fitting the curve in the paramagnetic region, we can observe that $(M/H)^{-1}$ deviates from the Curie – Weiss law below $1.16T_C$, $1.21T_C$ and $1.22T_C$ respectively for x = 0.1, 0.15 and 0.2, which signals the onset of short-range FM correlations.

Fig. 5 shows the deduced T_C values as a function of the $\langle r_A \rangle$. The Curie temperature decreases systematically with the increase of $\langle r_A \rangle$. Generally the Curie temperatures increase/decrease with the increase/decrease of $\langle r_A \rangle$ [22–25] and the relationship between T_C and $\langle r_A \rangle$ is due to the linkage between $\langle r_A \rangle$ and the ⟨Mn-O-Mn⟩ bond angle *i.e.* the variation of the ⟨Mn-O-Mn⟩ with x is not important in our system. In this case we have considered the effect of the average ⟨Mn-O⟩ distance which control the Jahn – Teller effect on the variation of T_C. Fig. 5 shows that the T_C decreases with the increase of ⟨Mn-O⟩. We concluded that the physics of our system is primarily dominated by two competing mechanisms, the Jahn – Teller effect which tries to localize carriers and the double exchange which tries to delocalize carriers.

On the other hand, one observes a second transition at the

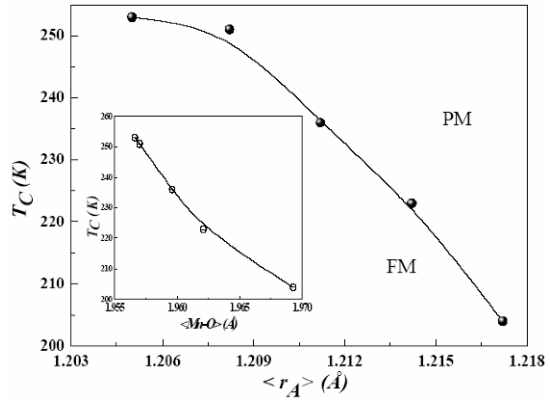

Figure 5. Curie temperature of the $La_{0.7}Ca_{0.3-x}Na_xMnO_3$ compounds as a function of $\langle r_A \rangle$. The paramagnetic (PM) and ferromagnetic (FM) regimes are indicated. Inset show Curie temperature as a function of the refined mean Mn – O bond length.

low temperatures that appears for $x \geqslant 0.1$ and behaves like an anomaly in FM state with decreasing amplitude with increase in x. This behavior is the same observed by B. Dabrowski [26] and that he assigns a charge ordering transition at $T_{CO,}$ a phenomenon that he explains by a decrease of the effective magnetic moment of the samples at low temperatures. This result of the apparition and the reduction amplitude of anomaly observed in low temperature in $M(T)$ is in agreement with the variation of σ_{JT}^2 for $x \geqslant 0.1$.

In fact, for $x = 0.1$, σ_{JT}^2 is maximal and the anomaly appears with higher amplitudes corresponding to a strong electron-phonon coupling arising for $x = 0.1$ from the Jahn-Teller distortion of the MnO_6 octahedra. For $x \geqslant 0.1$,σ_{JT}^2 decreases which implies a decrease of electron-phonon coupling and therefore the decrease of amplitude of observed anomalies in the $M(T)$ curves. Furthermore, the Jahn-Teller distortion is responsible for the decreases of the T_C [19]. Indeed the Jahn-Teller splitting of the $e_g(Mn)$ orbital is closely related to overlapping in the MnO_6 octahedra. An increased electron-phonon coupling is expected when the band width associated with the $e_g(Mn) - 2p_\sigma(O) - e_g(Mn)$ hybridization becomes narrower [27] and as result the (DE) is weakened. It is possible that a coupling between the lattice and magnetism via the Jahn-Teller distortion plays a role to the very sharp drop in the magnetization observed.

Table 2. The values of average ionic radius $\langle r_A \rangle$, variance of ionic radii σ^2, orthorhombic deformation D_O(%), octahedra distortion σ_{JT}^2, Curie temperature T_C, prefactor B from Bloch's law for different $La_{0.7}Ca_{0.3-x}Na_xMnO_3$ samples. ($^{IX}r_{La}^{3+}$ =1.216 Å; $^{IX}r_{Ca}^{2+}$ =1.18 Å; $^{IX}r_{Na}^{+}$ =1.24 Å) [21].

Composition	$\langle r_A \rangle$ (Å)	σ^2 ($\times 10^{-4}$ Å^2)	D_O ($\times 10^{-3}$%)	σ_{JT}^2 ($\times 10^{-4}$)	T_C (K)	B ($\times 10^{-5}$ K$^{3/2}$)
0	1.2052	2.72	0.193	2.399	253	1.14
0.05	1.2082	2.91	1.44	41.099	251	1.05
0.1	1.2112	2.93	1.98	43.827	236	3.62
0.15	1.2142	2.77	1.053	18.965	223	4.44
0.2	1.2172	2.43	0.53	8.62	204	7.28

In further substitutions of Ca for Na, reduction of Mn^{3+} content from 70% (*i.e.* the (DE) interaction is maximal in the manganite system when the ratio of Mn^{3+}/Mn^{4+} is near to 7/3) to 50%. This increased Mn^{4+} content will favor the Mn^{4+}- O^{2-}- Mn^{4+} super exchange interaction reducing the double-exchange (DE) interaction between Mn^{3+} - O^{2-}- Mn^{4+} that explains the reduction in the Curie temperature T_C.

The low- temperature thermal evolution of magnetization was fitted to Bloch's $T^{3/2}$ law [28] which can be written as

$$M(T,0)/M(0,0) = 1 - BT^{3/2} \qquad (3)$$

where$M(0,0)$ and $M(T,0)$ are the spontaneous magnetization at T = 0 K and at finite temperature, respectively and the prefactor B is a characteristic constant of the spin waves at low temperature [29] who can be written as

$$B = 2.612 \left(\frac{g\mu_B}{M(0)}\right)\left(\frac{k_B}{4\pi D}\right)^{3/2} \qquad (4)$$

where g is the Lande factor, μ_B is the Bohr magneton, k_B is the Boltzmann constant and D is the spin wave stiffens

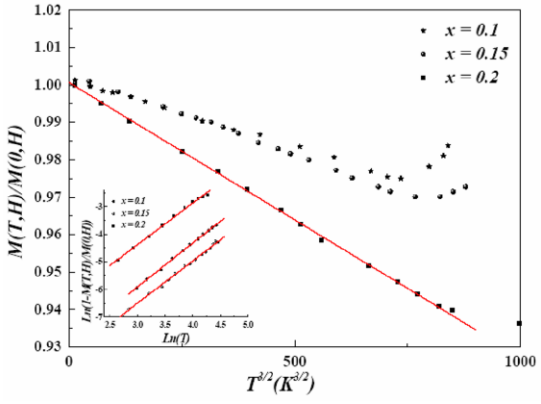

Figure 6. Plots of $M(T,H)/M(0,H)$, *vs.* $T^{3/2}$ fo $La_{0.7}Ca_{0.3-x}Na_xMnO_3$ for $x \geqslant 0.1$ at H = 0.1 T. The inset shows the $\mathrm{Ln}\big(1 - M(T,H)/M(0,H)\big)$ variation with $\mathrm{Ln}(T)$ to determine the slope of the linear fit to the data $\mathrm{Ln}\big(1 - M(T,H)/M(0,H)\big)$ *vs.* $\mathrm{Ln}(T)$. The solid line is a linear fit.

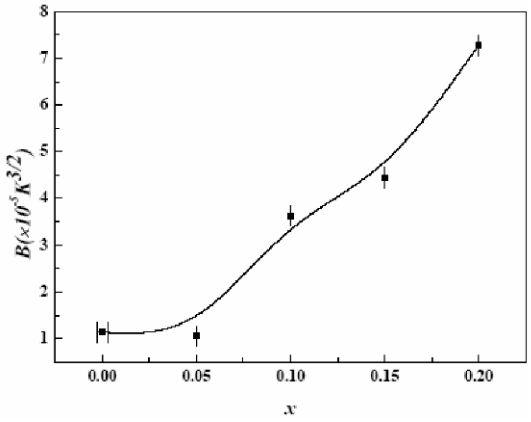

Figure 7. The variation of the prefactor B with x for $La_{0.7}Ca_{0.3-x}Na_xMnO_3$ systems.

constant. The stiffness D is defined by spin wave dispersion relation

$$E(q) = \Delta + Dq^2 \tag{5}$$

where $E(q)$ is the spin wave energy, $q$is the wave vector and Δ is the gap arising from anisotropy or applied magnetic field. In our analysis we assume $\Delta = 0$.

The curve $\mathrm{Ln}\big(1 - M(T,H)/M(0,H)\big)$ *vs.* $\mathrm{Ln}(T)$ in the inset of Fig. 6 is used to show that our compounds obey Bloch's $T^{3/2}$ law. It is predicted that the slope of the linear fit of the data $\mathrm{Ln}\big(1 - M(T,H)/M(0,H)\big)$ *vs.* $\mathrm{Ln}(T)$ must be close to 3/2. We found that slope is closer to 1.5 for all samples, only for $x = 0.1$ the slope is nearly 1.57 and therefore, the system $La_{0.7}Ca_{0.3-x}Na_xMnO_3$ belongs 3D Heisenberg class. Fig. 6 shows the reduced magnetization $M(T,H)/M(H,0)$ as a function of $T^{3/2}$ for $H = 0.1$ T for the system $La_{0.7}Ca_{0.3-x}Na_xMnO_3$ with $x \geqslant 0.1$. $M(H,0)$ was obtained by extrapolating $M(H,T)$ curves to $T = 0$ using a second order polynomial. The slope of the linear fit plot of the data $M(T,H)/M(H,0)$ vs. $T^{3/2}$ provided B values. The temperature range considered for fitting was 10 – 185 K for $x = 0$ and 0.05 compositions and 10 – 100 K for $x \geqslant 0.1$ compositions. B values are listed in Tab. 2. It can be seen that B is inversely proportional to $D^{3/2}$. It is well-known that D is directly proportional to the exchange integral A and the Curie temperature is directly proportional to the total exchange integral A [30].

Hence, from the experimental results of the decrease of the Curie temperature and the increase in values of $B$with x, plotted in the Fig. 7, it can be seen that the substitution of Ca by Na ions causes a decrease in total exchange integral A of the samples.

On the other hand, the value of B increases (D decrease) with increase of effective cationic radius $\langle r_A \rangle$ who is not in agreement with the result of N. Ghosh [31] showed that the spin stiffness constant D increases with increase of $\langle r_A \rangle$ in the system $La_{0.7-y}Nd_yPb_{0.3}MnO_3$, This contradiction is due to the variation in non monotonous of the variance σ^2 with $\langle r_A \rangle$ for our system. Hence, the thermal evolution of magnetization for the low- temperature in our system is influenced by the size mismatch σ^2.

4. Conclusion

In this work, we have investigated the crystal structure and magnetic properties of perovskite $La_{0.7}Ca_{0.3-x}Na_xMnO_3$ ($0 \leqslant x \leqslant 0.20$) compounds. There is no structural transition due to substitution of Ca^{2+} by Na^{+}. All the samples crystallize in an orthorhombic structure with the Pnma space group. Our study shows that the structural and magnetic properties depend strongly on the cation-size disorder parameter σ^2. For $x = 0.05$ and 0.10, σ^2 increases which causes a decrease of the cell parameter and the unit cell volume. On the other hand, we have found that σ^2 decreases for $x = 0.15$ and 0.20, which leads to an increase of the cell parameters. Magnetic measurements $M(T)$ show that our compounds exhibit a paramagnetic-ferromagnetic transition at T_C for $x = 0$ and 0.05. Therefore, the $M(T)$ curves reveal the presence of two types of magnetic transition for $x = 0.10$, 0.15 and 0.2. The first one is from the paramagnetic state to the ferromagnetic one at T_C. The second transition occurs at low temperature, indicating the presence of a charge ordered state. We have also found that as Ca^{2+} is progressively replaced by Na^{+} ions, the total exchange integral decreases causing a decrease

in the Curie temperature T_C.

References

[1] E. O. Wollan, W. C. Koehler, Phys. Rev. 100, 545 (1955)
[2] J. B. Goodenough, Phys. Rev. 100, 564 (1955)
[3] C. Zener, Phys. Rev. 82, 403 (1951)
[4] Myron B. Salamon, M. Jaime, Rev. Mod. Phys. 73, 583 (2001)
[5] J.M.D. Coey, M. Viret, S. von Molnar, Adv. Phys. 48, 167 (1999)
[6] P. Sciffer, A. P. Ramirez, W. Bao, S. W. Cheong, Phys. Rev. Lett. 75, 3336 (1995)
[7] P. W. Anderson, H. Hasegawa, Phys. Rev. 100, 675 (1955)
[8] V. N. Smolyaninova et al., J. Magn. Magn. Mater. 248, 348 (2002)
[9] H. Y. Hwang, S. W. Cheong, P. G. Radaelli, M. Marezio, B. Batlogg, Phys. Rev. Lett. 75, 914 (1995)
[10] L. M. Rodriguez-Martinez, J. P. Attifield, Phys. Rev. B 54, R15622 (1996)
[11] L. M. Rodriguez-Martinez, J. P. Attifield, Phys. Rev. B 58, 2426 (1998)
[12] Y. Tomioka, Y. Tokura, Phys. Rev. B 70, 014432 (2004)
[13] K. F. Wang et al., Appl. Phys. Lett. 88, 152505 (2006)
[14] K. F. Wang et al., Phys. Rev. B 73, 134411 (2006)
[15] B. Raveau, A. Maignan, C. Martin, M. Hervieu, Chem. Mater. 10, 2641 (1998)
[16] J. P. Attfiled, Chem. Mater. 10, 3239 (1998)
[17] P. V. Vanitha, P. N. Santosh, R. S. Singh, C.N.R. Rao, J. P. Attfield, Phys. Rev. B 59, 3184 (1996)
[18] A. J. Millis, P. B. Littlewood, B. I. Shraiman, Phys. Rev. Lett. 74, 5144 (1995)
[19] C. N. R. Rao, B. Raveau, Colossal Magnetoresistance, Charge Ordering and Relative Properties of Magnetic oxides (World Scientific, Singapore, 1998)
[20] R. A. Young, The Rietveld Method (Oxford University Press, New York, 1993)
[21] R. D. Shanon, Acta Cryst. A. 32, 751 (1976)
[22] Soma Das, T.K. Dey, Mater. Chem. Phys.108, 220 (2007)
[23] M. Bejar, E. Dhahri, E. K. Hlil, S. Heniti, J. Alloy. Compd. 440, 36 (2007)
[24] N. Rama, V. Sankaranarayanan, M. Opel, R. Gross, M.S. Ramachandra Rao, J. Alloy. Compd. 443, 7 (2007)
[25] Md. Motin Seikh, L. Sudheendra, C. N. R. Rao, Solid. State. Sci. 6, 561 (2004)
[26] B. Dabrowski et al., Phys. Rev. B 60, 7006 (1999)
[27] J. L. García-Muñoz et al., Phys. Rev. B 55, 668 (1997)
[28] C. Kittel, Quantum Theory of Solids (Wiley, New York, 1993)
[29] F. E. Luborsky, Ferromagnetic Materials (Elsevier, Amsterdam, 1979)
[30] B. X. Gu, S. Y. Zhang, H. C. Zhang, B. G. Shen, J. Magn. Magn. Mater. 204, 45 (1999)
[31] N. Ghosh et al., Phys. Rev. B 70, 184436 (2004)